# Product speciation during regeneration of lean NOx traps

*R. S. Larson, Sandia National Laboratories, Livermore, CA*
*J. A. Pihl, V. K. Chakravarthy, C. S. Daw, Oak Ridge National Laboratory, Oak Ridge, TN*

## Abstract

A set of elementary surface reactions is proposed for modeling the chemistry in a lean NOx trap during regeneration (reduction of stored NOx). The proposed reaction mechanism is based on a series of flow reactor temperature ramp experiments performed on a core sample from a fully formulated lean NOx trap catalyst. The experiments used simultaneous flow of NOx and reductant species ($H_2$ and CO) to decouple the reduction reactions from the NOx storage and release processes. The mechanism accounts for the observed product distribution (including $NH_3$ and $N_2O$) from the trap over a range of temperatures and inlet gas compositions similar to those expected for realistic operation. The mechanism includes many reactions already discussed in the literature, together with some hypothesized reactions that are required to match observations from the experiments. Preliminary results indicate that the NOx trap regeneration and byproduct formation rates can be effectively captured by using a relatively compact set of elementary reactions.

## Introduction

Control of NOx emissions from diesel or lean burn gasoline engines is a considerable technical barrier that must be overcome if the fuel efficiency advantages of these engines are to be fully realized. NOx storage-reduction catalysts (NOx traps) and urea-based selective NOx reduction catalysts are currently the leading candidate technologies under consideration for lean NOx control. In NOx traps, NOx is removed from the exhaust and stored over alkali or alkaline-earth metal oxides in the form of nitrites and nitrates during normal lean operation. Periodically, brief reducing conditions are imposed on the NOx trap (either from rich engine operation or direct post-engine fuel injection) to generate reductants such as CO, $H_2$, and hydrocarbons. These reductants stimulate NOx release/desorption (by decomposing nitrites and nitrates) and then catalytically reduce the released NOx. The desired reduction product is $N_2$, but it is also possible to form byproducts such as $N_2O$ and $NH_3$, which are themselves pollutants if released to the atmosphere. In addition, because reduction involves a direct fuel penalty, it is important to utilize the reductants as efficiently as possible. Furthermore, hybrid catalyst systems such as NOx trap/SCR combinations require the ability to predict the NOx trap effluent to effectively design the integrated system. Thus, it is critical to understand the chemical reactions and operating conditions leading to byproduct formation during the regeneration step.

Many prior studies have focused on the lean chemistry of NOx traps [1–18], but relatively few studies [5, 11, 15, 19–23] have addressed the regeneration phase. Even among the latter, little attention has been given to reduction product selectivity, specifically the formation of $N_2O$ and $NH_3$. This state of affairs prompted the work described in the present paper.

## Experiments

The experimental apparatus, procedure, and results are described in detail elsewhere [24]. Briefly, the measurements were made with a monolith core sample of circular cross section (0.875 inch diameter) from a commercial NOx trap supplied by Umicore Autocat USA Inc., with a washcoat specifically formulated for application with gasoline direct injection (GDI) engines. The washcoat contained $\gamma$-$Al_2O_3$, BaO and $ZrO_2$-$Ce_2O_3$, along with the noble metals Pt, Pd and Rh in the ratio 82:26:6 and at a total loading of 3990 g/m³. This particular NOx catalyst has been selected by the

LNT Focus Group of the DOE Crosscut Lean Exhaust Emissions Reduction Simulations (CLEERS) activity as a reference material for future collaboration (www.cleers.org).

As described in [24], the key reaction rate measurements were made under pseudo-steady-state and near-isothermal conditions during slow temperature programmed sweeps (at 5°C/minute) between 50°C and 500°C in a bench reactor. Prior to making the measurements, special procedures were implemented to bring the catalyst to a fully reduced state, so that the observed rates reflected primarily the adsorption, desorption, and reduction reactions on the noble metal components. The inlet gas typically included simulated exhaust quantities of $N_2$, $CO_2$, and $H_2O$ along with varying combinations of $H_2$, CO, and NOx (as NO or $NO_2$). NOx species were held at a concentration of 500 ppm, while the reductant concentrations were varied from 500 to 5000 ppm, yielding NOx/reductant ratios in a range from 1:1 to 1:10. Experiments were also performed with $NH_3$ or $N_2O$ in the feedgas to identify possible secondary reactions of these byproducts. The total flow rate was adjusted to give a space velocity of 100,000 $hr^{-1}$ for the 0.5 inch long core sample being used. Integral conversions of the various species at the catalyst exit were tracked with two chemiluminescent NOx analyzers and a Fourier Transform Infrared (FTIR) spectrometer. A schematic of the experimental setup is shown in Figure 1.
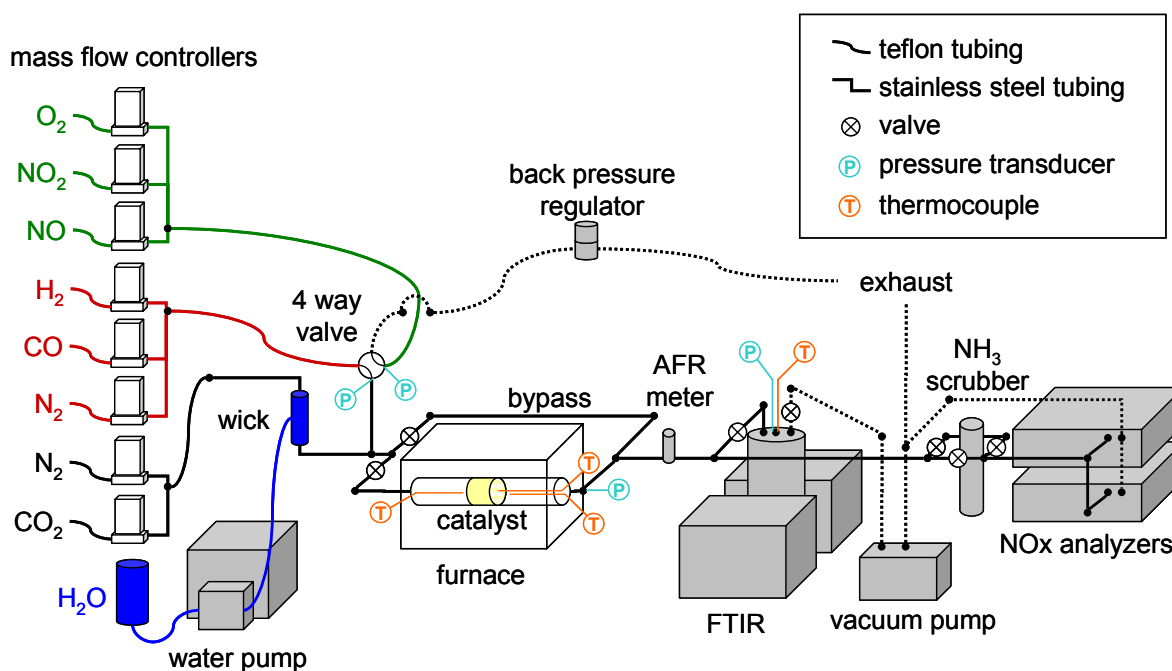


Figure 1. Schematic of experimental setup.

## Reactor Modeling

Because the experimental rate measurements were taken in an integral reactor, it was necessary to utilize an integral reactor model to relate the observations to the kinetic parameters associated with hypothesized reaction sets. We made this connection initially by utilizing the steady-state plug flow reactor code PLUG that is part of the Chemkin package [26]. For initial estimates we also assumed that boundary layer mass transfer was rapid relative to the surface reaction rates, and thus that the observed rates were kinetically controlled and could be computed directly with the Chemkin Arrhenius parameters.

For each set of inlet conditions, we used the plug flow model to compute steady state exit concentrations for all species at intervals of 50°C between 100°C and 500°C. By comparing the model predictions with the observed concentrations for all measured species in all 21 temperature

ramp experiments, we were then able to adjust the hypothesized reaction set and its associated Arrhenius parameters iteratively in order to improve the overall agreement between the simulations and the data. The iteration process was guided by a simple objective function based on the weighted norm of the deviation between predicted and observed values.

All of the rate parameters (pre-exponential factors, sticking coefficients, and activation energies) associated with the proposed mechanism were allowed to vary during the fitting process, which utilized the DAKOTA software package developed at Sandia National Laboratories to guide the optimization. If the rate parameters for a particular reaction in our mechanism were available in the literature (as in [6, 28, 29]), then those values were used as initial estimates for the optimization procedure.
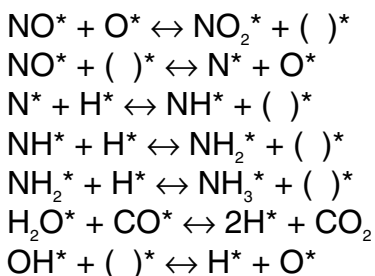
After the initial optimization, the resulting kinetic rates were used in a more detailed transient one-dimensional plug flow reactor model that also included bulk-to-wall heat and mass transfer. First, constant-temperature simulations were run for several selected cases over a long period of time in order to determine the asymptotic (steady) conversions with transport resistances included. The actual temperature ramps were then simulated as a means of checking the pseudo-steady state approximation. These results demonstrated good agreement with the simpler steady-state model, confirming the earlier assumptions of chemical kinetics control and isothermal steady-state behavior over the range of the experiments.
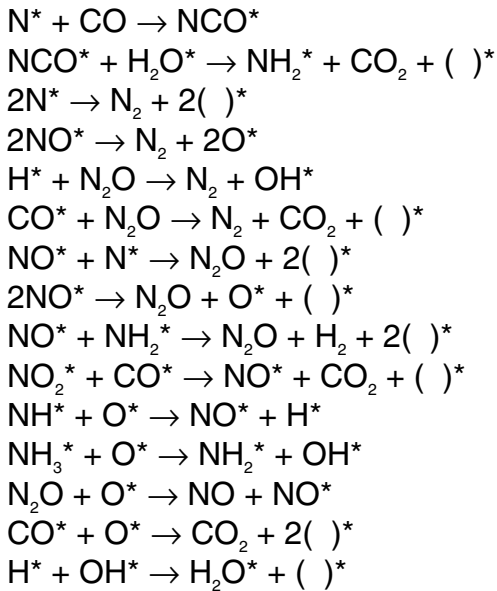
## Chemical Mechanisms

As noted previously, the Umicore catalyst is formulated with three noble metals (Pt, Pd and Rh) along with BaO (for storing NOx) and $Ce_2O_3$-$ZrO_2$ (for storing $O_2$). There are 10 gas phase species ($O_2$, NO, $NO_2$, CO, $H_2$, $CO_2$, $N_2$, $H_2O$, $N_2O$, and $NH_3$) whose evolution needs to be tracked along the length of the catalyst as they interact with the various surface intermediates. In order to make the problem more manageable, we assume that the combined effect of the three noble metal sites can be captured by metal sites of a single kind, typified by Pt. In general it is necessary to account for adsorption, desorption, dissociation, recombination, and atom-transfer reactions on these sites.

In nearly all of the experiments, the catalyst encounters only net rich flows, so storage of NOx and $O_2$ on the catalyst is assumed to be negligible. We further assume that the storage sites (in whatever form they may be) do not affect the kinetics on the noble metal sites. Therefore, we track only the chemistry occurring on catalytic noble metal sites using the following 13 surface species: $O^*$, $NO^*$, $NO_2^*$, $CO^*$, $H^*$, $N^*$, $OH^*$, $H_2O^*$, $NH^*$, $NH_2^*$, $NCO^*$, $NH_3^*$, and empty sites denoted by $(\ )^*$.

Through repeated comparisons of the observed exit concentrations with predictions of the plug flow reactor model, using various combinations of reactions involving the above species, we have reached a preliminary proposed mechanism involving 14 reversible and 15 irreversible elementary reactions. Seven of the reversible reactions account for simple adsorption and desorption of all gas phase species except $N_2$, $CO_2$, and $N_2O$. Among the gas phase species that adsorb, $O_2$ and $H_2$ are assumed to do so dissociatively. The remaining 7 reversible reactions are:

$NO^* + O^* \leftrightarrow NO_2^* + (\ )^*$
$NO^* + (\ )^* \leftrightarrow N^* + O^*$
$N^* + H^* \leftrightarrow NH^* + (\ )^*$
$NH^* + H^* \leftrightarrow NH_2^* + (\ )^*$
$NH_2^* + H^* \leftrightarrow NH_3^* + (\ )^*$
$H_2O^* + CO^* \leftrightarrow 2H^* + CO_2$
$OH^* + (\ )^* \leftrightarrow H^* + O^*$

The irreversible reactions in the mechanism are as follows:

$N^* + CO \rightarrow NCO^*$
$NCO^* + H_2O^* \rightarrow NH_2^* + CO_2 + (\ )^*$
$2N^* \rightarrow N_2 + 2(\ )^*$
$2NO^* \rightarrow N_2 + 2O^*$
$H^* + N_2O \rightarrow N_2 + OH^*$
$CO^* + N_2O \rightarrow N_2 + CO_2 + (\ )^*$
$NO^* + N^* \rightarrow N_2O + 2(\ )^*$
$2NO^* \rightarrow N_2O + O^* + (\ )^*$
$NO^* + NH_2^* \rightarrow N_2O + H_2 + 2(\ )^*$
$NO_2^* + CO^* \rightarrow NO^* + CO_2 + (\ )^*$
$NH^* + O^* \rightarrow NO^* + H^*$
$NH_3^* + O^* \rightarrow NH_2^* + OH^*$
$N_2O + O^* \rightarrow NO + NO^*$
$CO^* + O^* \rightarrow CO_2 + 2(\ )^*$
$H^* + OH^* \rightarrow H_2O^* + (\ )^*$

Note that formation of $N_2$ from any source is assumed to be irreversible and that reduction of $N_2O$ leads directly to $N_2$, thus preventing its eventual conversion to $NH_3$. The inclusion of reactions involving the formation and hydrolysis of $NCO^*$ to generate precursors to $NH_3$ is supported by the fact that when using only CO as a reductant, $NH_3$ is observed in the outflow at temperatures far below the light-off temperature of the water-gas shift reaction that produces $H_2$. In addition, recent experimental studies [5, 15] have confirmed the presence of an $NCO^*$ species on the surface.

## Results and Discussion

Because of the large number of experiments and simulations that were carried out (a total of 21 temperature ramps were performed), it is not possible to include a comprehensive review of the results here, so we have instead attempted to show some representative highlights. A more detailed discussion can be found in recently published studies [24,25], and additional results will be presented after further mechanism refinements now underway are completed.

Figures 2(a-d) show the measured and predicted exit concentrations of N-containing species and CO as functions of the inlet temperature in two experiments with NO and $H_2$ in the feedgas. The first experiment has a 1:1 molar ratio of NO and $H_2$, which corresponds to the stoichiometry for N2 formation. The second experiment uses a 1:2.5 mixture of NO and $H_2$, the same as the stoichiometric ratio for $NH_3$ production. These figures give a striking illustration of the degree to which product speciation depends on temperature and the ratio of NOx to reductant. For both experiments, low temperatures yield a mixture of reduction products. At moderate to high temperatures, the reduction reactions are quite selective. When the mixture is stoichiometric for $N_2$ formation, $N_2$ is the primary product. The selectivity shifts dramatically toward $NH_3$ when more reductant is added to the feed. This trend is even more pronounced when a 1:10 ratio of NOx to H2 is used (results not show here).

The temperature intervals within which $N_2O$ and $NH_3$ are formed in the reactor are well predicted by the model in the 1:1 case (figure 2(b)). However, when the $H_2$ concentration is increased to 1250 ppm, release of $NH_3$ is not observed in the model until the temperature reaches nearly 150°C (figure 2(d), while in the experiment $NH_3$ release begins at a temperature about 50°C lower (figure 2(c)).
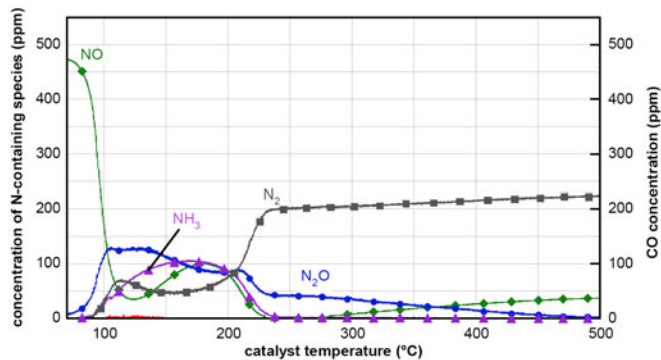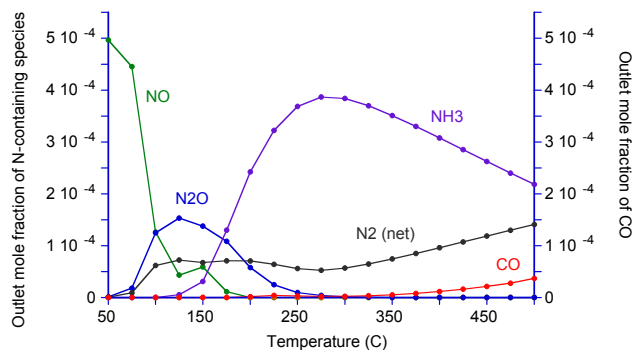
(a) 500 ppm NO/500 ppm H₂ experimental measurements
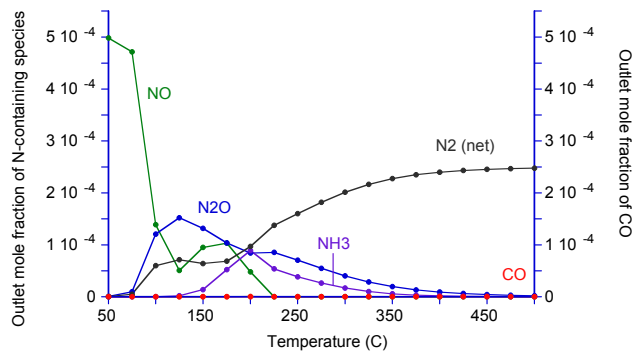
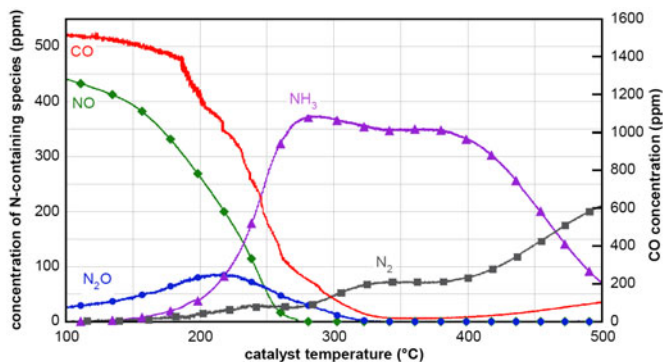(b) 500 ppm NO/500 ppm H₂ model predictions
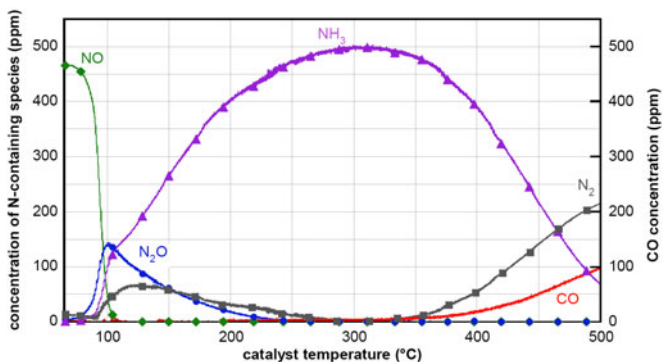
(c) 500 ppm NO/1250 ppm H₂ experimental measurements

(d) 500 ppm NO/1250 ppm H₂ model predictions

Figure 2. Variation of product species with inlet temperature for the experiments with 500 ppm NO and 500 ppm H2 (a and b) and 500 ppm NO and 1250 ppm $H_2$ (c and d).

Figure 3(a) shows results for an experiment with CO as the reductant. The results of this and the other CO experiments (not show here) are surprisingly similar to the corresponding $H_2$ cases. The product speciation is a strong function the NOx/CO ratio, with a 1:1 mixture generating primarily $N_2$ and higher levels of CO driving the selectivity toward $NH_3$. Also, low temperatures lead to a mixture of products, while moderate temperatures tend to drive the reactions to a single product. As illustrated in Figure 3(b), the amount of $NH_3$ released and the temperature interval where its breakthrough is observed are well predicted by the model.
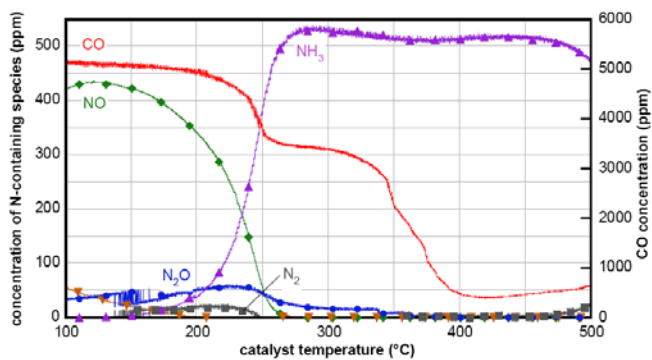


(a) experimental measurements
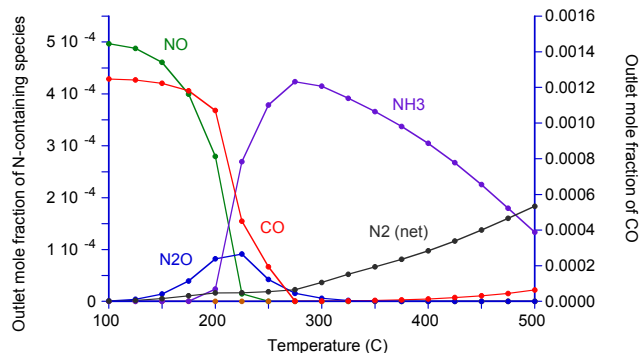
(b) model predictions

Figure 3. Variation of product species with inlet temperature: 500 ppm NO and 1250 ppm CO.

Changing the NOx species to $NO_2$ has negligible impact on the trends in product speciation. Figure 4(a) shows that a large excess of CO (1:10 ratio) drives the reduction of $NO_2$ completely to $NH_3$. The model results and data continue to match well with NO2 and high levels of reductant, as seen in figure 4(b). In this case, there is a distinct two-step drop in the experimental CO level that is well reproduced by the model. The two steps correspond to CO consumption by NCO* formation and the water-gas shift reaction, respectively. The production of $NH_3$ through formation of the NCO* intermediate is also well captured.
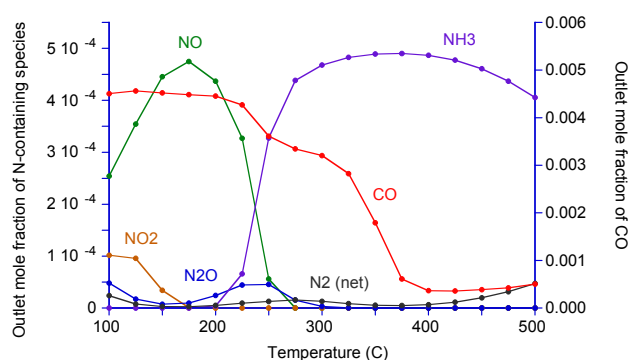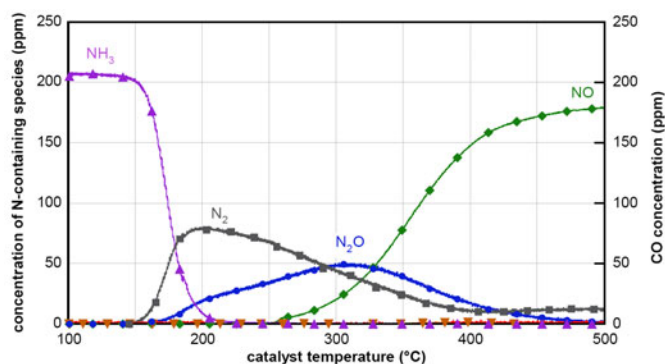


(a) experimental measurements (b) model predictions

Figure 4. Variation of product species with inlet temperature: 500 ppm $NO_2$ and 5000 ppm CO.

The results from one of the $NH_3$ oxidation experiments and the corresponding simulation are shown in Figure 5. $NH_3$ is readily oxidized by $O_2$ over the entire operating range of the catalyst. Once again, the product speciation is strongly dependent on the catalyst temperature, with $N_2$ the primary product at low temperatures, $N_2O$ becoming more predominant at moderate temperatures, and NO produced almost exclusively at high temperatures. The oxidation of $NH_3$ at low concentrations of $O_2$ is predicted extremely well by the model. These secondary byproduct reactions could be critical in predicting the actual outlet product concentrations of an operating NOx trap since a real world device will operate in an integral fashion and may have internal spatial variations in both gas phase and surface species that could lead to widely varying reactivities in different portions of the catalyst. For example, early in the regeneration process $NH_3$ could be formed near the front of the catalyst where the reductant concentration is high and then react with stored $O_2$ or NOx downstream to form $N_2O$. The proposed mechanism should be able to capture this type of behavior.
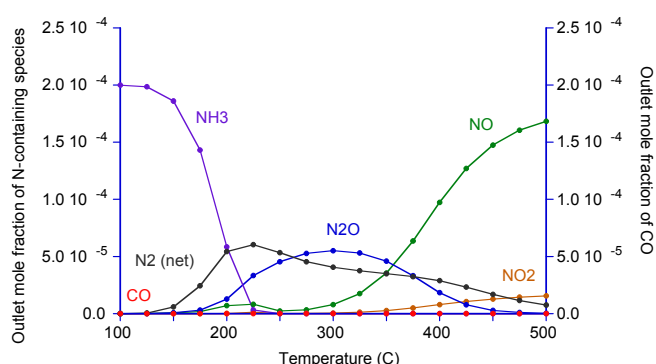


(a) experimental measurements (b) model predictions

Figure 5. Variation of product species with inlet temperature: 200 ppm $NH_3$ and 400 ppm $O_2$.

## Conclusions and Future Work

The following conclusions can be drawn about the current state of the kinetic mechanism for lean NOx reduction:

- NOx trap regeneration can be simulated with a reasonably compact set of elementary reactions.

- Regeneration product speciation depends heavily on both catalyst temperature and local reactant concentrations (in particular, the ratio of NOx to reductant).

- The model tends to be less successful at low temperatures, especially with regard to NOx reduction by $H_2$.

- Both water-gas shift and isocyanate pathways are needed to explain the observed patterns of CO consumption during reduction of NOx.

- The kinetics of the reactions in the mechanism, rather than boundary layer transport resistances, seem to limit the interspecies conversion in the reactor.

- The use of pseudo-steady state simulations for the slow temperature ramps appears to be reasonable, at least for purposes of parameter optimization.

We plan to refine the above mechanism further in order to overcome the shortcomings that have been noted here. One key feature that has been missing from the analysis thus far is the imposition of thermodynamic (i.e., equilibrium) constraints on the kinetic parameters during the optimization procedure. Work toward this end is underway. Obviously, the current mechanism also needs to be augmented with surface reactions involving species on $BaO/BaCO_3$ sites before it can describe a complete lean/rich cycle.

In spite of the above shortcomings, we believe that the mechanism presented here constitutes a major advance over what has previously been available. Most importantly, we have demonstrated that it is possible to simulate the steady-state production of $NH_3$ and $N_2O$ over a realistic range of exhaust compositions (including $H_2O$ and $CO_2$) and temperature for a commercial catalyst using a relatively compact elementary reaction set. We expect that such detailed mechanisms will prove much more generally useful in the long run than ad hoc empirical global mechanisms for simulating NOx traps.

## References

1. N. Takahashi, H. Shinjoh, T. Iijima, T. Suzuki, K. Yamazaki, K. Yokota, H. Suzuki, N. Miyoshi, S. Matsumoto, T. Tanizawa, T. Tanaka, S. Tateishi, and K. Kasahara. *Catalysis Today*, 27:63–69, 1996.
2. H. Mahzoul, J. F. Brilhac, and P. Gilot. *Applied Catalysis B: Environmental*, 20:47–55, 1999.
3. J. A. Anderson, A. J. Paterson, and M. Fernandez-Garcia. In *12th International Congress on Catalysis*, volume 130, pages 1331–1336, Amsterdam, The Netherlands, 2000. Elsevier Science B. V.
4. E. Fridell, H. Persson, B. Westerberg, L. Olsson, and M. Skoglundh. *Catalysis Letters*, 66:71–74, 2000.
5. H. Y. Huang, R. Q. Long, and R. T. Yang. *Energy & Fuels*, 15:205–213, 2001.

6. L. Olsson, H. Persson, E. Fridell, M. Skoglundh, and B. Andersson. *J. Phys. Chem. B*, 105:6895–6906, 2001.
7. F. Prinetto, G. Ghiotti, I. Nova, L. Lietti, E. Tronconi, and P. Forzatti. *J. Phys. Chem. B*, 105:12732–12745, 2001.
8. B. Westerberg and E. Fridell. *Journal of Molecular Catalysis A*, 165:249–263, 2001.
9. N. W. Cant and M. J. Patterson. *Catalysis Today*, 73:271–278, 2002.
10. I. Nova, L. Castoldi, L. Lietti, E. Tronconi, and P. Forzatti. *Catalysis Today*, 75:431–437, 2002.
11. L. Olsson, E. Fridell, M. Skoglundh, and B. Andersson. *Catalysis Today*, 73:263–270, 2002.
12. D. Uy, K. A. Wiegand, A. E. O'Neill, A. Dearth, and W. H. Weber. *J. Phys. Chem. B*, 102:387–394, 2002.
13. K. Chakravarthy, C. S. Daw, and K. E. Lenox. *SAE paper 2003-01-3246*, 2003.
14. C. S. Daw, K. E. Lenox, K. Chakravarthy, W. E. Epling, and G. Campbell. *International Journal of Chemical Reactor Engineering*, 1, 2003.
15. L. Castoldi, I. Nova, L. Lietti, and P. Forzatti. *Catalysis Today*, 96:43–52, 2004.
16. W. S. Epling, J. E. Parks, G. C. Campbell, A. Yezerets, N. W. Currier, and L. E. Campbell. *Catalysis Today*, 96:21–30, 2004.
17. I. Nova, L. Castoldi, L. Lietti, E. Tronconi, P. Forzatti, F. Prinetto, and G. Ghiotti. *Journal of Catalysis*, 222:377–388, 2004.
18. Y. Su and M. D. Amiridis. *Catalysis Today*, 96:31–41, 2004.
19. L. Lietti, P. Forzatti, I. Nova, and E. Tronconi. *Journal of Catalysis*, 204:175–191, 2001.
20. H. Mahzoul, P. Gilot, J. F. Brilhac, and B. R. Stanmore. *Topics in Catalysis*, 16:293–298, 2001.
21. D. James, E. Fourre, M. Ishii, and M. Bowker. *Applied Catalysis B: Environmental*, 45:147–159, 2003.
22. S. Poulston and R. R. Rajaram. *Catalysis Today*, 81:603–610, 2003.
23. Z. Liu and J. A. Anderson. *Journal of Catalysis*, 224:18–27, 2004.
24. J. A. Pihl, J. E. Parks, C. S. Daw, T.W. Root. *SAE paper 2006-01-3441*, 2006.
25. R. S. Larson, V. K. Chakravarthy, J. A. Pihl, C. S. Daw. *SAE paper 2006-01-3446*, 2006.
26. R. J. Kee, F. M. Rupley, J. A. Miller, M. E. Coltrin, J. F. Grcar, E. Meeks, H. K. Moffat, A. E. Lutz, G. Dixon-Lewis, M. D. Smooke, J. Warnatz, G. H. Evans, R. S. Larson, R. E. Mitchell, L. R. Petzold, W. C. Reynolds, M. Caracotsios, W. E. Stewart, and P. Glarborg. *CHEMKIN Collection*, Release 3.5, Reaction Design, Inc., San Diego, CA, 1999.
27. J. S. Choi, W. P. Partridge, and C. S. Daw. *Applied Catalysis A: General*, 293:24–40, 2005.
28. J. H. B. J. Hoebink, R. A. van Gemert, J. A. A. van den Tillaart, and G. B. Marin. *Chemical Engineering Science*, 55:1573–1581, 2000.
29. G. C. Kolstakis and A. M. Stamatelos. *AIChE Journal*, 45:603–614, 2004.